frontiers | Frontiers in Chemistry

TYPE Mini Review
PUBLISHED 12 December 2022
DOI 10.3389/fchem.2022.1063288

OPEN ACCESS

EDITED BY
Jinwen Shi,
Xi'an Jiaotong University, China

REVIEWED BY
Xianliang Fu,
Wuhan Institute of Technology, China

*CORRESPONDENCE
Rashid Mehmood,
rashidm066@yahoo.com
Zia Ahmad,
Mianzia909@gmail.com

†These authors have contributed equally to this work

SPECIALTY SECTION
This article was submitted to Photocatalysis and Photochemistry, a section of the journal Frontiers in Chemistry

RECEIVED 07 October 2022
ACCEPTED 25 November 2022
PUBLISHED 12 December 2022

CITATION
Mehmood R, Ahmad Z, Hussain MB, Athar M, Akbar G, Ajmal Z, Iqbal S, Razaq R, Ali MA, Qayum A, Chishti AN, Zaman Fu, Shah R, Zaman S and Adnan (2022), 2D–2D heterostructure g-C_3N_4-based materials for photocatalytic H_2 evolution: Progress and perspectives. *Front. Chem.* 10:1063288. doi: 10.3389/fchem.2022.1063288

2D–2D heterostructure g-C_3N_4-based materials for photocatalytic H_2 evolution: Progress and perspectives

Rashid Mehmood[1*†], Zia Ahmad[2*†], Muhammad Bilal Hussain[3], Muhammad Athar[1], Ghulam Akbar[2], Zeeshan Ajmal[4], Sikandar Iqbal[5], Rameez Razaq[6], Mohammad Arif Ali[7], Abdul Qayum[8], Aadil Nabi Chishti[5], Fakhr uz Zaman[9], Rahim Shah[10], Shahid Zaman[11] and Adnan[10]

[1]Institute of Chemical Sciences, Bahaudin Zakariya University, Multan, Pakistan, [2]Department of Chemistry and Biochemistry, University of Agriculture, Faisalabad, Pakistan, [3]School of Energy and Power Engineering, Shandong University, Jinan, China, [4]Department of Soil and Environmental Science, University of Agriculture, Faisalabad, Pakistan, [5]ZJU-Hangzhou Global Technological and Innovation Center, Zhejiang University, Hangzhou, China, [6]Department of Chemical Engineering, Norwegian University of Science and Technology (NTNU), Trondheim, Norway, [7]Institute of Chemistry, The Islamia University of Bahawalpur, Bahawalpur, Pakistan, [8]Department of Chemistry, Shantou University, Shantou, China, [9]School of Materials Science and Engineering, University of Jinan, Jinan, China, [10]Institute of Chemical Sciences University of Swat, Swat, Khyber Pakhtunkhwa, Pakistan, [11]Department of Mechanical and Energy Engineering, Southern University of Science and Technology (SUTech), Shenzhen, China

Photocatalytic hydrogen generation from direct water splitting is recognized as a progressive and renewable energy producer. The secret to understanding this phenomenon is discovering an efficient photocatalyst that preferably uses sunlight energy. Two-dimensional (2D) graphitic carbon nitride (g-C_3N_4)-based materials are promising for photocatalytic water splitting due to special characteristics such as appropriate band gap, visible light active, ultra-high specific surface area, and abundantly exposed active sites. However, the inadequate photocatalytic activity of pure 2D layered g-C_3N_4-based materials is a massive challenge due to the quick recombination between photogenerated holes and electrons. Creating 2D heterogeneous photocatalysts is a cost-effective strategy for clean and renewable hydrogen production on a larger scale. The 2D g-C_3N_4-based heterostructure with the combined merits of each 2D component, which facilitate the rapid charge separation through the heterojunction effect on photocatalyst, has been evidenced to be very effective in enhancing the photocatalytic performance. To further improve the photocatalytic efficiency, the development of novel 2D g-C_3N_4-based heterostructure photocatalysts is critical. This mini-review covers the fundamental concepts, recent advancements, and applications in photocatalytic hydrogen production. Furthermore, the challenges and perspectives on 2D g-C_3N_4-based heterostructure photocatalysts demonstrate the future direction toward sustainability.

KEYWORDS

photocatalytic H2 evolution, two dimensional, graphitic carbon nitride, heterojunction, sustainable energy

Introduction

Energy, along with environmental issues, has become increasingly important in recent decades; however, renewable energy alternatives such as wind or solar energy are essential to lessen the provoked global energy shortage (Hou et al., 2013; Qi et al., 2017; Zhu et al., 2018; Zhao et al., 2021; Ran et al., 2022). In various catalytic processes, 2D g-C_3N_4 layered composite materials are effective catalysts because of their visible range (2.7 eV) band gap, wavelength (~460 nm), photo-responsive character, special geometry, and the presence of numerous N-based molecules to stabilize the metal nanoparticles. Furthermore, 2D g-C_3N_4 also have the ability to produce coordinative unsaturated metal centers than their 3D counterparts, which are sometimes even more active and stable than 3D or 1D materials (Yan et al., 2016; She et al., 2017; Wang et al., 2020; Tran Huu et al., 2021). Interestingly, the conduction band (CB) bottom of g-C_3N_4 (−1.13 eV) is more negative as compared to the water reduction potential (H_2, 0 V), whereas the uppermost valence band (VB) is in a slightly higher positive state than the water oxidation potential (O_2). Hence, g-C_3N_4 can be utilized for water oxidation (WOR) in addition to the reduction of water (HER) (Yang et al., 2018; Wang et al., 2020). However, the g-C_3N_4 demonstrates constrained photocatalytic efficiency in terms of low activity as the electron and hole pairs show rapid recombination (Wang et al., 2009; Wang et al., 2014a; Wang et al., 2017; Huang et al., 2019). That is the reason that the g-C_3N_4 only performs photocatalytic HER to only a limited μmoles per gram per hour and is even less activated for water oxidation. Overall, nitrogen atoms in g-C_3N_4 are at an ideal oxidation position for water to O_2 molecule, and the C atom serves as an active site for H^+ ion for the generation of H_2 (Wang et al., 2011; Ong et al., 2016). It should be noted that an effective approach to substantially enhance the photocatalytic activity of g-C_3N_4 material is to investigate the carbon and nitrogen atoms substitution as porous surfaces in 2-dimensional g-C_3N_4. Nevertheless, the challenge of rapid recombination of electron and hole pairs and excitonic characteristics continued to restrict the efficiency of the g-C_3N_4 photocatalysts. To further improve the photocatalytic efficiency of g-C_3N_4, and to overcome the problem of rapid electron and hole pairs recombination, various strategies, including structural engineering (Liu et al., 2018), surface modification (Liu et al., 2020), forming composites or heterostructure with other semiconductors (Zheng et al., 2020), doping of metals and non-metals (Wang et al., 2017), or the co-catalysts have been investigated.

The most effective strategy is to construct the heterostructure/heterojunction involving 2D g-C_3N_4 and 2-dimensional material for the spatial departure of photo-generated electron and hole pairs (Fu et al., 2019; Yuan et al., 2019). The formation of heterojunction of two-dimensional designed structures along with the highly intact interface is among the key factors which usually support the electronic cloud transmission between the two materials (Ran et al., 2018b; Yang et al., 2018). In addition, the ultrathin nanosheets of 2D heterostructure produce an abundant catalytic active site, which decreases the transfer distance and improves the light absorption capacity. Moreover, the 2D heterostructure photocatalysts are exceptionally stable. That is why constructing multiple 2D materials to create 2D/2D heterostructure photocatalysts has recently gained considerable interest (Su et al., 2019; Sun et al., 2019). Moreover, photo-catalytically induced electron–hole pair clouds of g-C_3N_4 may be amended and deviate from the exciton severance in g-C_3N_4. Thus, these generated electron holes may be separated enough to improve the 2D g-C_3N_4 photocatalytic action. Different dimensions of photocatalysts are shown in Figure 1.

Basic mechanism of photocatalytic water splitting

The semiconductor material excited by light irradiation of more intensity or band gap equivalent intensity drives the photocatalytic H_2O splitting. During this scenario, electron flow takes place from the VB to the CB, whereas the hole (h^+) remains in the VB of the material. The photo-generated electrons (e^-) and holes (h^+) potentially reduce H^+ and oxidize the H_2O. In this case, if the bottom of CB is more negative relative to the H^+ ion reduction potential, it can be a suitable candidate for water reduction. As illustrated in Figure 2A, the VB value should be greater than the H_2O molecule's oxidation potential to generate an O_2 molecule (1.23 eV vs. NHE at pH = 0). Furthermore, the semiconductor band gap value should be greater than the thermodynamic requirement of 1.23 eV, and it must span the redox potential of H_2O in order to be a viable candidate for one-step excitation water splitting (Hisatomi et al., 2014). Recombining the photoinduced electronic pair clouds can happen in bulk and during a photocatalytic H_2O response to the bulk catalyst surface. Recombination of electron and hole pairs may reduce the photocatalyst performance.

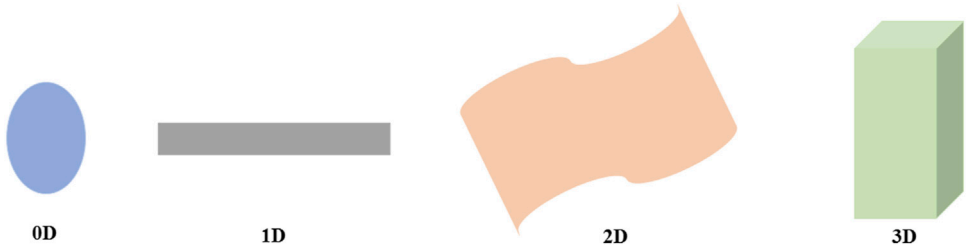

FIGURE 1
Schematic representation of photocatalysts relative to the different dimensions.

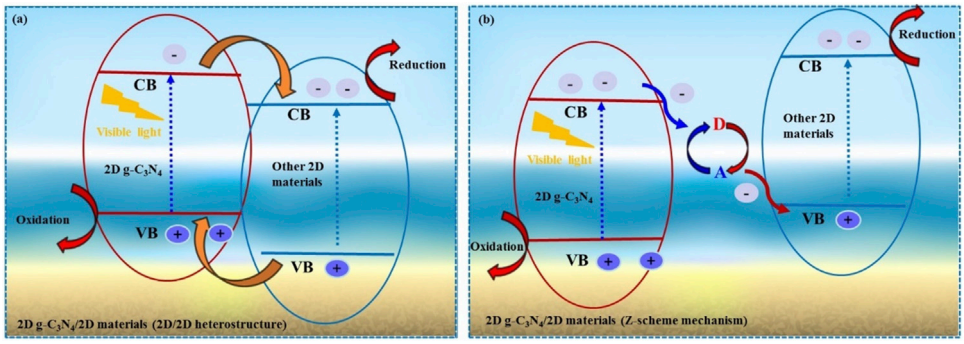

FIGURE 2
Schematic illustration of fundamental of photocatalytic water splitting for 2D g-C_3N_4 based 2D-2D heterostructure photocatalysts. **(A)**, type-II photocatalytic mechanism, **(B)** Z-scheme mechanism. CB (conduction band), VB (valance band); Eg, (band gap).

Z-scheme

In 1979, the traditional Z-scheme photocatalyst was proposed (Bard, 1979). The components of this photocatalytic system are two photocatalysts and a redox couple. The redox couple consists of an electron acceptor (A) and an electron donor (D), including I_3^-/I^{-1} and Fe^{+3}/Fe^{+2}. In the conventional Z-scheme mechanism (Figure 2B), photogenerated electrons in the CB of 2D g-C_3N_4 react with A to form D, while photogenerated holes in the VB of other 2D catalysts react with D to form A. As a result, the electrons in other 2D catalysts CB and the holes in 2D g-C_3N_4 VB are preserved. However, traditional Z-scheme mechanisms have limitations and drawbacks. Due to the necessity of redox ion pairs, traditional Z-scheme photocatalysts are only applicable in the solution phase.

S-scheme

The S-scheme heterojunction, which is comprised of an oxidation photocatalyst (OP) and a reduction photocatalyst, was proposed to overcome the inadequacy of traditional type-II heterojunction and Z-scheme heterojunction (RP) (Xu et al., 2020). Overall, the S-scheme mechanism vividly describes the charge transfer pathway in heterojunction photocatalysts, but it is also consistent with the scientific principles and experimental phenomena. The S-scheme heterojunction photocatalyst has both high charge separation efficiency and potent redox capability. As anticipated, it has received a great deal of attention since its proposal. Numerous sources discuss the fabrication and photocatalytic performance of 2D/2D g-C_3N_4-based S-scheme heterojunction photocatalysts (g-C_3N_4/BiOBr) (Zhang et al., 2021).

This mini-review focuses on significant and advanced phenomena in engineering 2D g-C_3N_4-based heterostructure photocatalysts, particularly for hydrogen production. The main aspects of 2D g-C_3N_4 heterogeneous photocatalysts often provide some rising strategies for contriving various 2D heterostructure photocatalysts. Further, it also provides an understanding of the designs of g-C_3N_4-based heterogeneous catalysts, along with special attention to the underlying mechanism of photocatalyzed recombination of electron–hole pairs. Moreover, the recent advancement and challenges of

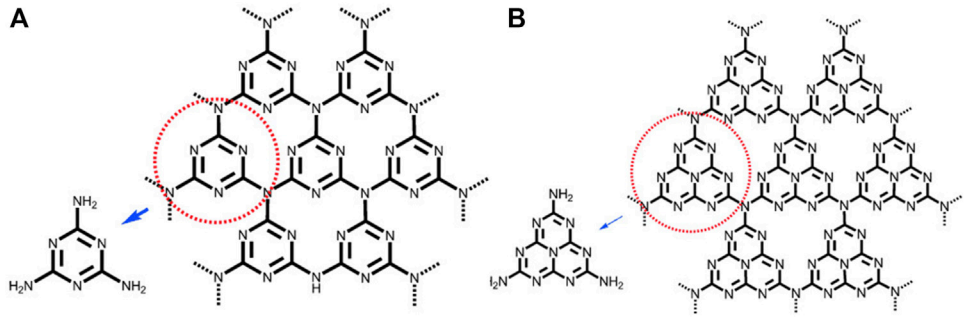

FIGURE 3
(A) Triazine and **(B)** tri-s-triazine (heptazine) structures of g-C_3N_4 (gray, blue, and white balls are carbon, nitrogen, and hydrogen, respectively) (Wang et al., 2012), Copyright 2012 Wiley Online Library.

g-C_3N_4-based heterostructure photocatalysts for H_2 production have subsequently been highlighted. Finally, a brief overview of 2D heterogeneous photocatalysts relevant to water reduction (H_2 evolution) or water oxidation (O_2 evolution) Z-scheme is described, and the current state of science and key questions are addressed.

Structure and properties of g-C_3N_4

Melamine, melon, melam, and melem are recognized as heptazine and triazine-based molecular compounds, whereas the coplanar tri-s-triazine unit is regarded as the fundamental structural motif required to produce g-C_3N_4. As shown in Figure 3, the basic tectonic units of g-C_3N_4 are triazine (C_3N_3) and tri-s-triazine/heptazine (C_6N_7) rings. Unlike conventional organic semiconductor materials, g-C_3N_4 cases have large stability, including resistance to heat and chemicals. Thermal gravimetric analysis (TGA) and thermal gravimetric analysis (TG) on g-C_3N_4 indicate that it is non-volatile up to 600°C and will be nearly completely decomposed at 700°C. The flake-like structure of g-C_3N_4 is very similar to that of graphite, as is well known.

2D g-C_3N_4 as photocatalysts

Wang et al., for the first time, used g-C_3N_4 as visible light photocatalysts for hydrogen production (Wang et al., 2009). Graphitic carbon nitride was later discovered to absorb visible light owing to its 2.7 eV band gap value, which is consistent with a wavelength of 460 nm. Moreover, the CB of g-C_3N_4 in its bottommost is more negative relative to the H_2O reduction potential of the H_2 molecule. The valence band uppermost region is more positive as compared to the oxidation potential of water to O_2 molecule. So, graphitic carbon nitride applied as a photocatalyst could be a suitable candidate for H_2O splitting in visible light (Yan et al., 2016). It is very imperative to understand the band distance of g-C_3N_4 upsurges as the bulk graphitic carbon nitride flake off to monolayer by quantum confinement effect.

Principles of 2D g-C_3N_4-based 2D heterostructure photocatalysts

The basic principle to design the 2D heterostructure photocatalysts is to overwhelm the hole pair recombination issues in primeval g-C_3N_4. On the basis of continuous efforts, it is concluded that an appropriate heterogeneous structure is described as the utmost viable approach to increase the lifetime of electron–hole pair clouds that significantly improve the catalysts' photocatalytic efficiency. Overall, the 2D interface design strategy is essential for 2D photocatalysts and photocatalytic performance, as the synthesis methods determine the quality of the interface in the heterostructure materials.

Preparation of 2D g-C_3N_4-based heterostructure photocatalysts

The strategies to fabricate the 2D–2D g-C_3N_4-based hetero-structured photocatalysts Interfaces play a crucial role in the photocatalytic performance of the 2D photocatalysts, as the quality of the interface is determined by the construction strategy. To date, numerous effective fabrication techniques for the synthesis of 2D–2D g-C_3N_4-based heterostructure photocatalysts, such as ultrasonic absorption (Zhang et al., 2018; Ayodhya and Veerabhadram, 2020), hydrothermal method (Tian et al., 2013), electrostatic self-assembly (Ma et al., 2017; Wang et al., 2022), and chemical vapor deposition (Zhang and Fu, 2018), have been extensively studied.

Nonetheless, one of the simplest ways to construct the 2D–2D g-C_3N_4-based heterostructure is to disperse the two distinct 2D components in the solution *via* stirring or sonication to form a mixture. After drying the mixture in an oven to evaporate the solvents, the 2D–2D photocatalyst can be obtained. Using ultrasonic dispersion and drying, 2D–2D g-C_3N_4/N-doped $La_2Ti_2O_7$ layered heterostructures were fabricated. Nevertheless, these 2D–2D interfaces were successfully fabricated by a weak interaction between two 2D components, and the 2D components were easily separated during the photocatalysis process (Cai et al., 2017b). However, using a hydrothermal method, this issue can be resolved. For instance, g-C_3N_4/$ZnIn_2S_4$ (Manchala et al., 2019) and TiO_2-g-C_3N_4 (Zhang et al., 2017) heterostructure photocatalysts, *etc.,* have been prepared by the hydrothermal method, and numerous intimate interfaces were formed between the g-C_3N_4 and the second counterparts. The heterointerface junctions not only enhance the stability but also enhance the generation of electron–hole pairs and inhibit their recombination. Overall, the hydrothermal method is an energy-efficient and environmentally friendly method because the reaction occurs under closed system conditions. Furthermore, the hydrothermal method is kinetically slow at all temperatures, making it easy to control. To further enhance the kinetics of crystallization, a microwave–hydrothermal method was also developed. For instance, TiO_2/g-C_3N_4 heterostructures were created by a simple microwave–hydrothermal process, which demonstrated enhanced photocatalytic H_2 production activity compared to TiO_2 (Girish et al., 2022). Additionally, electrostatic self-assembly is a viable technique for fabricating intimate 2D–2D interfaces. Notably, surface charge modification plays a significant role in the engineering of 2D–2D photocatalysts with intimate interfacial contact using this method (Ma et al., 2017; Wang et al., 2022). To achieve electrostatic self-assembly, the surface charges on various 2D photocatalysts must be modified to obtain opposing charges (i.e., positive and negative charges). Notably, the zeta potential value can be used to calculate the photocatalyst's charge. For instance, to form the 2D/2D g-C_3N_4/rGO by electrostatic self-assembly, the g-C_3N_4 was protonated by concentrated H_2SO_4 and HNO_3 under mild ultrasonication to obtain the positively charged surface; the measured zeta potential value was +37.2 mV (Vinesh et al., 2020). With the aid of ultrasonication and agitation, the g-C_3N_4/rGO intimate interface was obtained. In addition, the stacking interactions between the sp^2 lattices of g-C_3N_4 and the sp^2 graphene lattices, as well as the hydrogen-bonding interactions between the nitrogen-containing groups in g-C_3N_4, are advantageous for electrostatic self-assembly. Due to the intimate interface and the introduction of rGO, the hydrogen production rate of g-C_3N_4/rGO (557 mol g^{-1} h^{-1}) was significantly higher than that of g-C_3N_4 (158 mol g^{-1} h^{-1}). Furthermore, the construction of the 2D/2D g-C_3N_4/rGO by electrostatic self-assembly facilitates the photocatalytic reduction of carbon dioxide to methane. Chemical vapor deposition (CVD) is also an efficient method for constructing 2D/2D heterostructures with intimate interfaces, such as intraplane and interplane interfaces (Zhang and Fu, 2018). Typically, in the CVD method, gas molecules are injected into a reaction chamber that has been heated to a specific temperature. For instance, the CVD-fabricated intraplane Fe_2O_3/g-C_3N_4, type-II InSe/g-C_3N_4 heterostructure, and g-C_3N_4/TiO_2 exhibited excellent optoelectronic and photovoltaic performance (Wang et al., 2014b). Yuanzhi Hong produced Ta_2O_5/g-C_3N_4 heterojunctions using a straightforward, one-step heating procedure. Under visible-light irradiation (>420 nm) (Hong et al., 2017), the photocatalytic activity of as-prepared photocatalysts was determined by splitting water for hydrogen evolution under visible-light irradiation. Compared to pure g-C_3N_4, the obtained heterojunctions demonstrated significantly enhanced hydrogen production. The heterojunction of 7.5% TO/CN exhibited the highest photocatalytic hydrogen evolution efficiency, which was approximately 4.2 times that of pure g-C_3N_4. In addition, the 7.5% TO/CN sample exhibited excellent photochemical stability even after 20 h of photocatalytic testing. Although CVD is a powerful technique for the synthesis of 2D/2D materials, the gaseous byproducts of the process are typically extremely toxic. Moreover, using the CVD method to synthesize 2D materials on a large scale remains a formidable challenge.

2D layered g-C_3N_4-based hetero-structured photocatalysts for H_2 production

As described earlier, in 2009, Wang et al. first discovered that 2D layered g-C_3N_4, along with featuring a 2.7 eV band gap value, is a favorable photocatalyst utilizing visible light for H_2 production. After that, many researchers have devoted their attention to the synthesis of 2D heterostructure photocatalysts with 2D g-C_3N_4, as proper band construction is an important deliberation in electing the second semiconductor for engineering g-C_3N_4-based heterostructure photocatalysts. For example, Di et al. (2014) investigated g-C_3N_4/BiOI heterostructure photocatalysts through a simple hydrothermal approach; schematic representation is illustrated in Figure 4A. Transmission electron microscopy demonstrates the 2D morphology of C_3N_4/BiOI heterostructure (Figure 4B), and HRTEM images show the different crystal fringes patterns, which corresponds to the g-C_3N_4 layered structure and BiOI structure (Figure 4C). A clear interface between g-C_3N_4 and BiOI could be seen in Figure 4C. The intimate interface between the two constituents is helpful to transfer the charge along the interfaces. BiOI constitutes the band gap (1.94 eV), which displays a decent photo response in the visible spectrum of

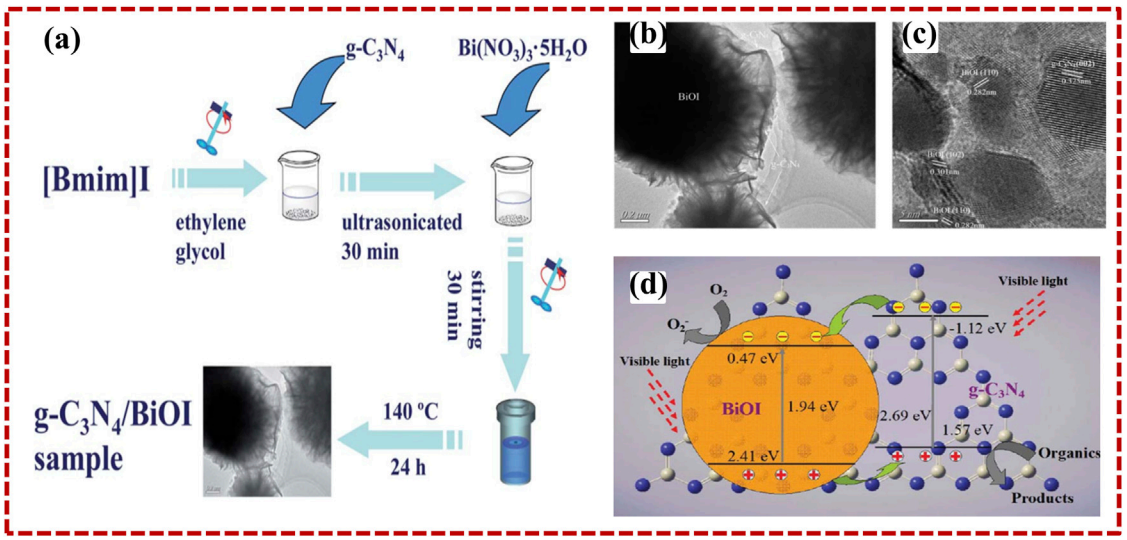

FIGURE 4
The synthesis method **(A)**, TEM **(B)**, and HRTEM **(C)** pictures of g-C_3N_4/BiOI. **(D)** The transferring mechanism of the photo-generated charge carriers across g-C_3N_4/BiOI nanocomposites. Reprinted with permission from Di et al. (2014), Copyright 2014 Royal Society of Chemistry.

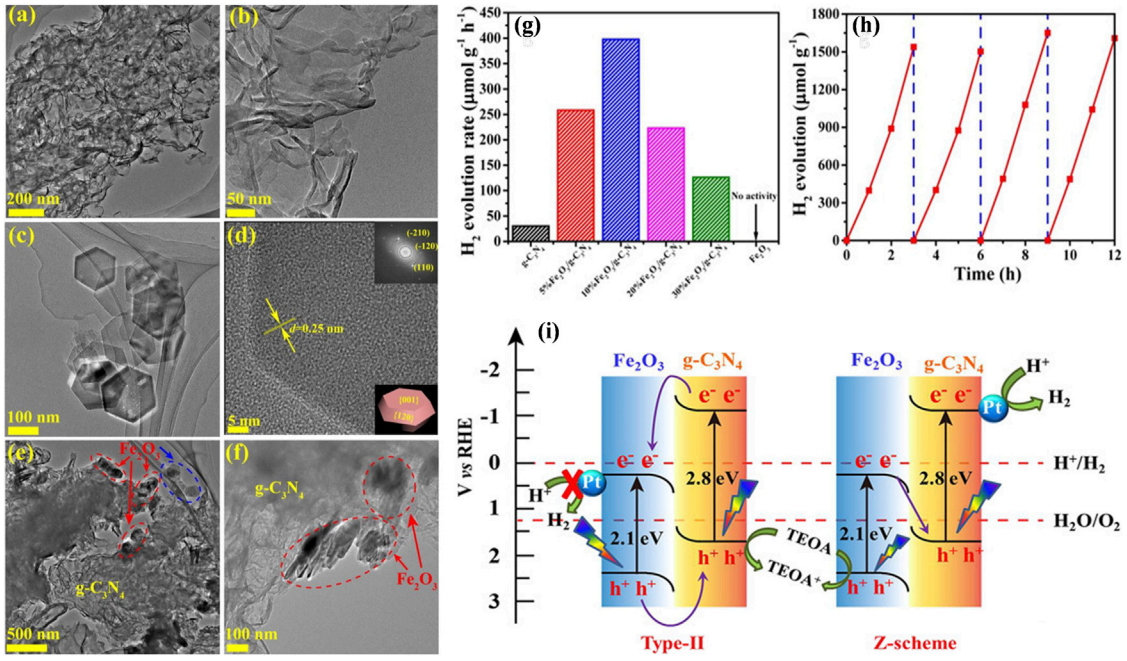

FIGURE 5
TEM photos of 2D Fe_2O_3/g-C_3N_4 **(A,B)** and 2D g-C_3N_4 **(C)**. HRTEM image of Fe_2O_3 **(D)** and the samples with 10% Fe_2O_3/g-C_3N_4 **(E,F)**. The upper right corner inset part of the image **(D)** shows Fe_2O_3 nanoplate FFT pattern; in contrast, the lower right corner is a depiction of Fe_2O_3 nanoplate facets. **(G)** Photocatalytic activities demonstration by g-C_3N_4 nanosheets, Fe_2O_3, and 2D Fe_2O_3/g-C_3N_4 heterostructure, **(H)** the stability of 10% sample Fe_2O_3/g-C_3N_4 heterostructure with visible-light of $\lambda > 420$ nm irradiation, **(I)** Charge transfer mechanism of traditional type-II heterojunction and direct Z-scheme. Reproduced with permission from Xu et al. (2018), Copyright 2018 Wiley Online Library.

light (Figure 4D). Owing to the appropriate band placement of g-C_3N_4 and BiOI, the photo-induced hole–electron pair may be powerfully separated to operate the photocatalytic reaction.

Later on, Xu et al. (2018) employed a facile electrostatic self-assembly method to synthesize a 2D Fe_2O_3/g-C_3N_4 heterostructure photocatalyst. A robust interaction was observed among Fe_2O_3 and g-C_3N_4, originating from the transition and separation of electron and hole pair charges.

Interestingly, the movement of charges through the 2D Fe_2O_3/g-C_3N_4 interface was found suitable for the Z-scheme. Therefore, Fe_2O_3/g-C_3N_4 photocatalysts were applied for direct photocatalytic water splitting through Z-scheme with visible-light irradiation using Pt as a co-catalyst. The morphology of the 2D Fe_2O_3/g-C_3N_4 heterostructure is depicted in Figure 5. As can be studied by the TEM in Figures 5A,B, the Fe_2O_3/g-C_3N_4 heterostructure exhibited 2D morphology. The exfoliated g-C_3N_4 reveals a morphology similar to curled-veil, stated as typical flexible nanosheets (Figure 5C). The FFT profile reveals the presence of six identical (1 2 0) spots, corresponding to the (0 0 1) basal plane up and the (0 0 1) basal plane down, implying that a crystal fringe distance of 0.25 nm represents (1 2 0) planes (Figure 5D). Consequently, the lower right corners of Figures 5E,F display the typical structure of a hexagonal nanoplate made of Fe_2O_3 with exposed facets. Based on the Fe_2O_3 and g-C_3N_4 morphologies, the TEM images with 10% Fe_2O_3/g-C_3N_4 show hexagonal nanoplate (red and blue circles in Figures 5E,F), which represents Fe_2O_3, while curled nanosheets were identified as g-C_3N_4. The nanoplates of Fe_2O_3 are predominantly accumulated on the edges of g-C_3N_4, promoting the establishment of an interface of the heterostructure. The effectiveness of the photocatalysts was assessed by their H_2O splitting ability to produce hydrogen using visible light as an irradiation source. Triethanolamine (TEOA) was utilized to scavenge the holes. The nanoparticles of Pt played the role of co-catalysts, which were accumulated on the photocatalyst surface through *in situ* photoreduction. Figure 5G demonstrates that pristine Fe_2O_3 performs a very poor H_2 generation performance, whereas g-C_3N_4 exhibited mild photocatalytic hydrogen generation at a 30.1 mmol h^{-1} g^{-1} rate. Interestingly, the photocatalytic performance of the Fe_2O_3/g-C_3N_4 heterostructure for the H_2 evolution was found 398.0 mmol h^{-1} g^{-1}, almost 13-times that of the pristine g-C_3N_4. A detailed photocatalytic hydrogen generation mechanism on Fe_2O_3/g-C_3N_4 heterostructure is illustrated in Figure 5I. As shown in Figure 5I, photocatalytic systems primarily consider two possible pathways: the conventional type-II heterojunction and the direct Z-scheme system. As seen in Figure 5I (type-II), the CB and VB energies of g-C_3N_4 are 1.1 and 1.7 eV, respectively. While the CB and VB values of Fe_2O_3 are 0.3 and 2.4 eV, to be obtained from the empirical formula (Wang et al., 2015). However, due to the low CB value of Fe_2O_3, electrons cannot participate thermodynamically in the photocatalytic hydrogen evolution reaction. As shown in 4i (type-II), if the composite followed the traditional type-II mechanism, g-C_3N_4 would transfer to the CB of Fe_2O_3, while photogenerated holes would transfer from the VB of Fe_2O_3 to the VB of g-C_3N_4 when exposed to visible light. In this case, the photocatalytic activity of the composite should be less than that of g-C_3N_4. However, the actual experimental results showed that the photocatalytic activity of the composite Fe_2O_3/g-C_3N_4 is higher than that of g-C_3N_4. On the basis of the preceding results and data analysis, it is proposed that a direct Z-scheme charge transfer route can occur over Fe_2O_3/g-C_3N_4 composites, thereby enhancing the photocatalytic performance in H_2 production. In particular, when both Fe_2O_3 and g-C_3N_4 absorb photons with sufficient energy, electrons are excited from their respective VB to CB. As a result, the Fe_2O_3/g-C_3N_4 composites retain both the high oxidation ability of Fe_2O_3 and the high reduction ability of g-C_3N_4, thereby providing a substantial driving force for the water reduction reaction. The photogenerated electrons formed on the g-C_3N_4 surface would transfer to Pt NPs in order to participate in the surface water reduction for H_2 evolution, whereas the photogenerated holes collected on the Fe_2O_3 surface could be consumed in TEOA oxidation. This direct Z-scheme charge transfer process significantly improves charge separation efficiency and provides a large driving force for the photocatalytic water reduction reaction, thereby enhancing the performance of photocatalytic water splitting.

Recently, Zhong et al. (2018) developed a self-assembled 2D O-g-C_3N_4/TiO_2 heterostructure photocatalyst by single-pot solvothermal method for the H_2 evolution reaction (HER) with visible light photocatalytic radiations. The two-dimensional existence of each component of the heterostructure itself gives rise to broad, unique surface areas, a marked quantum containment effect, and exposed active sites. The 2D photos of O-g-C_3N_4/TiO_2 1:1 taken by HAADF-STEM reveal a fine heterostructure formation (Figure 6A). Element mapping performed with EDX reveals that the larger nanosheet is O-g-C_3N_4, and the small nanosheets around its border are TiO_2 (Figures 6B–F). In order to analyze the interface among the two elements, the electron energy loss spectra (EELS) were collected in separate contact regions 1 and 2, as well as in the virgin TiO_2 leaf areas, as shown in Figure 6G. Figure 6H displays the photocatalytic activity for HER on the 2D O-g-C_3N_4/TiO_2 with visible light irradiation. Electrons in the VB of O-g-C_3N_4 are excited to the CB by the incident photons with appropriate energy. TEOA trapped the photo-induced holes produced in the valence bands of O-g-C_3N_4, whereas photo-induced electrons passed from the heterojunction of covalent NeOeTi into the valence band of TiO_2 nanosheet.

Photo-induced electrons eventually enter into and evenly accumulate on the surface of TiO_2, a Pt co-catalyst, and the water splitting happens through electrons into H_2 gas. The heterojunction identified through NeOeTi linkage caused effective charge separation at the interface and the effect of

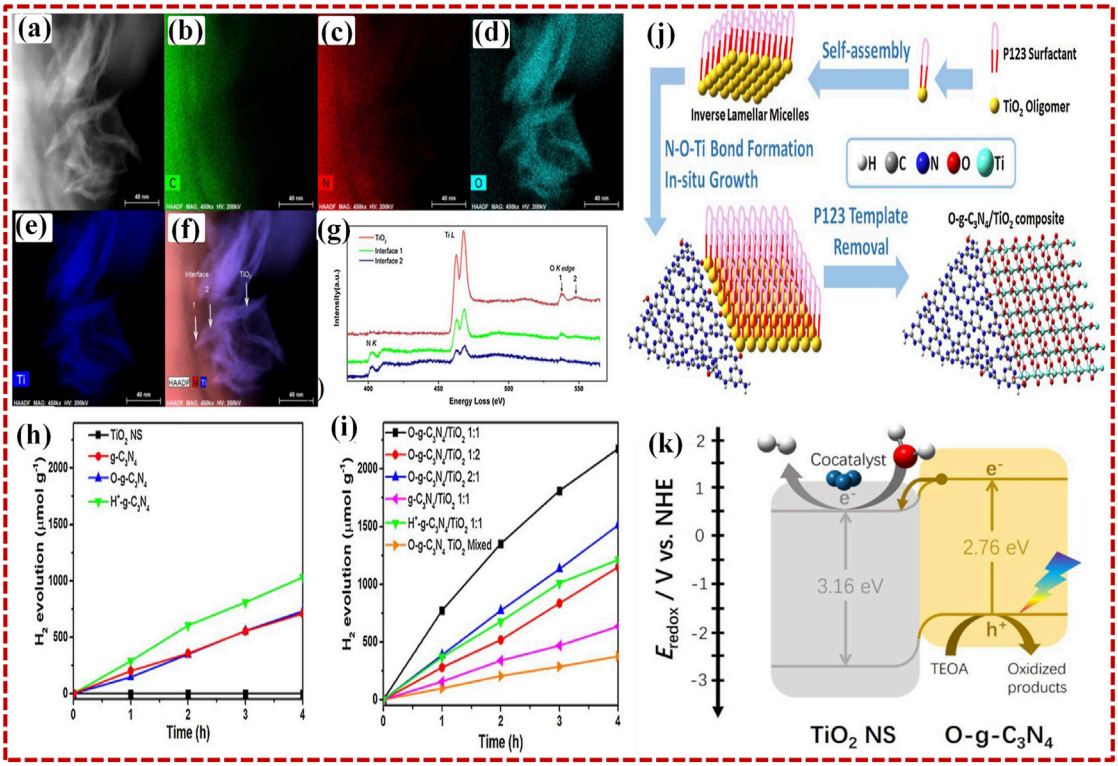

FIGURE 6
(A) Relevant HAADF-STEM picture and EDS elemental map of the respective regions of 2D O-g-C_3N_4/TiO_2 photocatalyst C **(B)**, N **(C)**, O **(D)**, and Ti **(E)**. **(F)** superposed N, Ti, and HAADF maps revealing the interface areas and TiO_2 leaves. **(G)** NK edge, Ti L edge, and O K edge as seen in EELS spectra of interface and TiO_2 region. **(H)** H_2 production plot vs. time of TiO_2 NS, g-C_3N_4, O-g-C_3N_4, H^+ - g-C_3N_4, and **(I)** composites of O-g-C_3N_4/TiO_2 at ratios of 1:1, 1:2, 2:1, 2D g-C_3N_4/TiO_2 (1:1), H^+ - g-C_3N_4/TiO_2 (1:1), and mixed O-g-C_3N_4 TiO_2 **(J)** scheme of the fabrication of O-g-C_3N_4/TiO_2 composite. **(K)** Suggested mechanism for photocatalytic H_2 production on O-g-C_3N_4/TiO_2 (1:1) composite using irradiation by visible-light. Reproduced with permission from Zhong et al. (2018), Copyright 2018 Elsevier.

band bending, which expanded the absorption range and enhanced the photocatalytic activity of 2D O-g-C_3N_4/TiO_2 heterostructure photocatalyst, as shown in Figure 6I.

Very recently, Jia et al. (2020b) reported that 2D 15% $FeSe_2$/CNNS heterostructure exhibits superior photocatalytic hydrogen generation performance (1655.6 μmol h^{-1} g^{-1}) with no co-catalyst in Na_2S/Na_2SO_3 aqueous medium and excellent stability for 12 h. In addition, it also demonstrated the simultaneous elimination of chromium (VI) and methylene blue (MB) using sunlight irradiation. Most notably, relative to conventional single-step four-electron reaction, $FeSe_2$/CNNS can trigger the photocatalytic H_2O splitting to hydrogen generation through a sequential two-electron, two-step reduction reaction based on capturing of active free radical and H_2O_2 sensing investigation. The efficiency is simultaneously realized by such 2D/2D inter-plane hetero-structures, as seen in Figure 7.

Here, we summarize 2D g-C_3N_4-based heterostructure photocatalysts and compounds that contain 2D g-C_3N_4. Table 1 lists the experimental conditions for photocatalytic water splitting and their photocatalytic performances by using different sacrificial reagents.

Role of the sacrificial agent

Overall, photocatalytic H_2 production from water using either UV-light-responsive photocatalysts or 2D g-C_3N_4-based visible-light-responsive photocatalysts is a low-efficiency process (Chen and Mao, 2007; Hong et al., 2013). This is primarily due to the high rates of electron and hole recombination induced by photoexcitation. To increase the efficiency of H_2 production from water splitting, electron donors are typically required to act as a sacrificial agent, consuming holes and preventing the recombination of photoinduced electrons and holes on the semiconductor surface. Common sacrificial electron donors include Na_2S–Na_2SO_3, methanol, triethanolamine, lactic acid, etc., and several studies have compared the H_2 production rates of photocatalysts using various sacrificial agents. For instance,

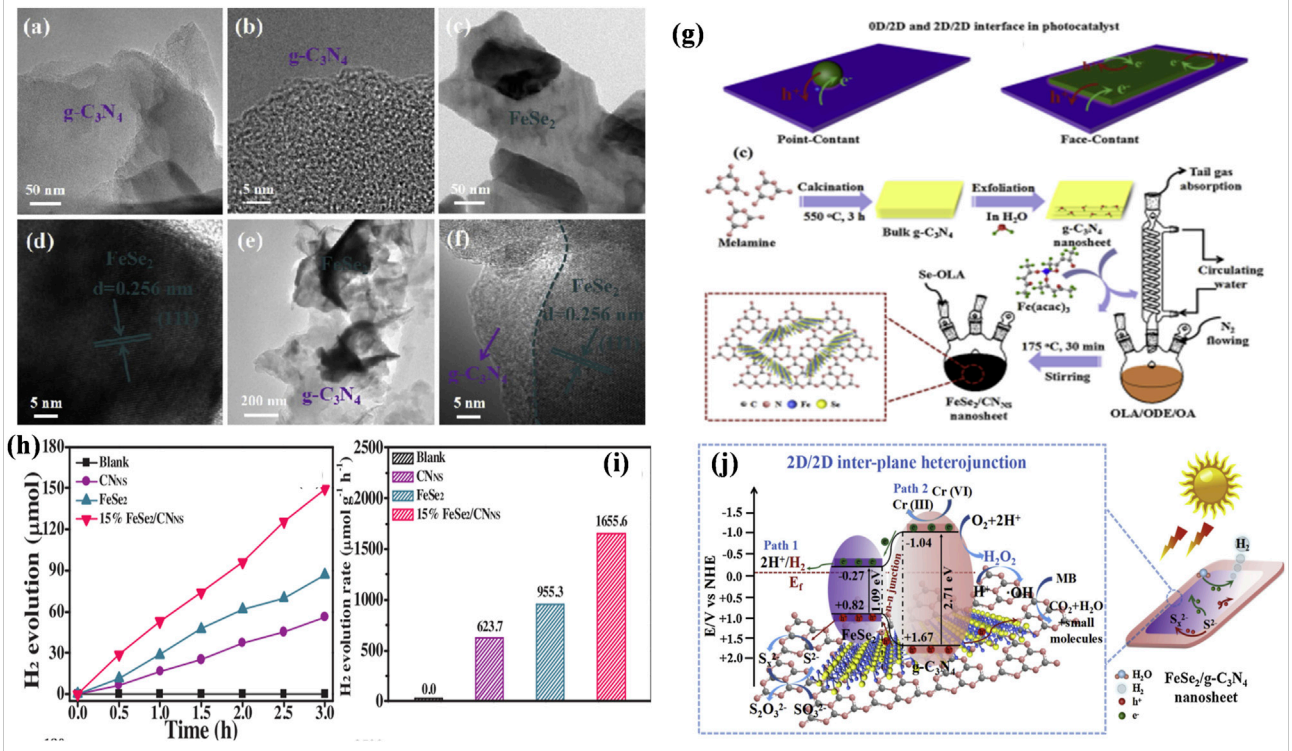

FIGURE 7
TEM image of pristine g-C_3N_4 **(A,B)**, $FeSe_2$ nanosheets **(C,D)**, and $FeSe_2$/CNNS composite of 15% sample **(E,F)**. Schematic image depicting the interfaces of **(G)** 0D/2D heterostructures, 2D/2D heterostructures and Schematic diagram for the fabrication process of inter-plane hetero-structures of 2D/2D $FeSe_2$/CNNS. Photocatalytic hydrogen evolution plot **(H)** and rates **(I)** of virgin g-C_3N_4, $FeSe_2$, and heterostructures of numerous $FeSe_2$/CNNS. **(J)** Schematic depiction of the charge carrier transport in 2D/2D $FeSe_2$/CNNS samples irradiated by sunlight. Reproduced with permission from Jia et al. (2020b), Copyright 2020 Elsevier.

Hong et al. examined the H_2 production performance of 2D g-C_3N_4/NiS (g-C_3N_4 as the photocatalyst and NiS as the co-catalyst) in solutions of triethanolamine, lactic acid, oxalic acid, and ascorbic acid. According to the results, the H_2 evolution rate for C_3N_4/NiS in triethanolamine was 48.2 mol h^{-1} g^{-1}, whereas the other three sacrificial agents did not support photocatalytic water splitting. These findings and other reports on photocatalysts indicate that sacrificial agents are indispensable for achieving high H_2 evolution rates. Some studies show that sacrificial agents play a role in the dispersion of noble metal nanoparticles (co-catalysts). It has also been determined that the sacrificial agents have a significant effect on the loading amount, particle size, and distribution of various metals on the surface of g-C_3N_4. For instance, in methanol solution, the actual loading amount of Pt and Au is greater than in triethanolamine solution. In the presence of methanol, the distribution and size of Pt nanoparticles are improved, whereas the distribution and size of Au nanoparticles are improved in the presence of triethanolamine. As a result, the Pt- and Au-decorated g-C_3N_4 photocatalysts synthesized exhibit notably distinct charge transfer properties, resulting in enhanced photocatalytic activities of the same g-C_3N_4 photocatalyst under diverse conditions (Cao et al., 2018).

Role of co-catalysts

Similarly, the recombination of photogenerated electron–hole pairs of g-C_3N_4 can be inhibited by loading the co-catalyst on the surface of g-C_3N_4. Briefly, co-catalysts can be categorized as singly loaded (noble-metal, metal with high abundance, and non-metallic) and co-loaded hybrid co-catalysts, which effectively promote the separation of photogenerated electron–hole and subsequently improve photocatalytic performance. Therefore, bimetallic, noble-metal co-catalysts, co-loading with different co-catalysts or one co-catalyst with various components, and the potential for solar-driven hydrogen evolution appear more promising.

Inspired by the rule of C and N in g-C_3N_4, also overall photocatalytic water splitting enhanced by the use of 2D g-C_3N_4-based hetero-structured photo-catalysts, as abundant interfaces between different components have gained attention for enhanced light absorption and facilitated photogenerated charge separation in the photo-catalysis. Recently, successful

TABLE 1 Selected reports on the 2D–2D g-C_3N_4-based heterostructure for photocatalytic H_2 production.

Photocatalysts	Sacrificial agent/co-catalyst	Applications	Catalyst amount/ solution composition	Quantum efficiency or hydrogen production	Light source	Ref
phosphorene/g-C_3N_4	lactic acid/Pt	H_2 production	20 mg/100 ml	1.2% at 420 nm	300 W xenon lamp/(λ > 400 nm	Ran et al. (2018a)
g-C_3N_4/NiFe-LDH	CH_3OH	H_2 production	30 mg/30 ml	1488 mmol^2 h^{-1}	125 W pressure Hg lamp (λ > 420 nm)	Nayak et al. (2015)
α- Fe_2O_3/g-C_3N_4	/RuO_2	H_2 production	10 mg/100 ml	44.35% at λ = 420 nm	300 W xenon lamp/(λ > 420 nm)	She et al. (2017)
2D g-C_3N_4/In_2Se_3	TEOA	H_2 production	20 mg/100 ml	4.8 mmol g^{-1}·h^{-1}	36 W LED lamp/(λ > 420 nm)	Zhang et al. (2020)
g-C_3N_4/N-$La_2Ti_2O_7$	CH_3OH	H_2 production	5 mg/5 ml	10.7% at 420 nm	Asahi Spectra, mW cm−2/ (λ > 420 nm)	Cai et al. (2017a)
WO_3.H_2O/g-C_3N_4	No sacrificial reagent	H_2 production	100 mg/100 ml	482 μmol g^{-1} h^{-1}	350 W xenon lamp/(λ > 420 nm)	Yang et al. (2018)
$FeSe_2$/g-C_3N_4	Na_2S/Na_2SO_3	H_2 production	100 mg/100 ml	1655.6 μmol·h^{-1}	300 W xenon lamp/(λ > 420 nm	Jia et al. (2020a)
O- g-C_3N_4/TiO_2	TEOA	H_2 production	50 mg/50 ml	587.1 μmol g^{-1} h^{-1}	300 W xenon lamp/(λ > 400 nm	Zhong et al. (2018)
g-C_3N_4/TiO_2	CH_3OH/ CH_3CH_2OH	H_2 production	0.15 g/100 ml	10,150 μmol h^{-1}	300 W xenon lamp	Fajrina and Tahir, (2019)
$Ba_5Nb_4O_{15}$/g-C_3N_4	oxalic acid/Pt	H_2 production	100 mg/100 ml	2.67 mmol h^{-1} g^{-1}	300 W xenon lamp/(λ > 400 nm	Wang et al. (2020)
ZnS/g-C_3N_4	Na_2S/Na_2SO_3	H_2 production	50 mg/100 ml	713.68 μmol h^{-1} g^{-1}	300 W xenon lamp/(λ > 420 nm	Hao et al. (2018)
$ZnIn_2S_4$/g-C_3N_4	TEOA	H_2 production	50 mg/60 ml	7.05% at 420 nm	300 W xenon lamp/(λ > 420 nm	Qin et al. (2020)
CdS/WS_2/CN.	Lactic acid	H_2 production	10 mg/100 ml	1174.5 mmol h^{-1} g^{-1}	300 W Xe (λ > 420 nm)	Zou et al. (2018)
NH_2-MIL-125(Ti)/ g-C_3N_4	TEOA	H_2 production	10 mg/100 ml	8.7 mmol g^{-1} h^{-1}	300 W xenon lamp/(λ > 420 nm	Xu et al. (2017)
Nb_2O_5/g-C_3N_4	TEOA/Pt	H_2 production	10 mg/100 ml	50.65% and 14.75% at 405 nm and 420 nm	300 W xenon lamp/(λ > 400 nm	Yi et al. (2021)
Mo_2C/g-C_3N_4	TEOA	H_2 production	5 mg/100 ml	6.7% at 420 nm	300 W xenon lamp/(λ > 420 nm	Zheng et al. (2020)
CdS/α- Fe_2O_3	Na_2S/Na_2SO_3	H_2 production	50 mg/100 ml	46.9% at 420 nm	300 W xenon lamp/(λ > 420 nm	Shen et al. (2020)
g-C_3N_4/Graphene/ MoS_2	TEOA	H_2 production	50 mg/250 ml	3.4% at 420 nm	300 W Xe (λ > 420 nm)	Yuan et al. (2018)
Nb_3O_7F/g-C_3N_4	10% TEOA	H_2 production	30 mg/1000 ml	1242.0 μmol h^{-1} g^{-1}	300 W Xe 300 nm ≤ λ ≤ 1100 nm	Li et al. (2021)
Mo_2C/g-C_3N_4	TEOA	H_2 production	20 mg/90 ml	675.27 μmol $h^{-1}g^{-1}$	300 W Xe lamp, λ > 400 nm	Liu et al. (2022)
g-C_3N_4/$ZnIn_2S_4$	40 ml, 10% lactic acid	H_2 production	8 mg/40 ml	10.92 mmol h^{-1} g^{-1}	300 W Xe lamp, λ > 420 nm	Dang et al. (2021)

(Continued on following page)

TABLE 1 (*Continued*) Selected reports on the 2D–2D g-C_3N_4-based heterostructure for photocatalytic H_2 production.

Photocatalysts	Sacrificial agent/co-catalyst	Applications	Catalyst amount/ solution composition	Quantum efficiency or hydrogen production	Light source	Ref
ReS_2/CCN	10% TEOA	H_2 production	20 mg/100 ml	3.46 mmol g^{-1} h^{-1}	The xenon lamp (300 W, 250 mW cm^{-2}) stimulated sunlight	Yang et al. (2022)
$LaVO_4$/CN	10 ml of FFA or TEOA	H_2 production	20 mg/100 ml	0.95 mmol g^{-1} h^{-1}	The xenon lamp (300 W, 250 mW cm^{-2}) stimulated sunlight	Li et al. (2022)
AgPd/2D g-C_3N_4	Formic acid/ Sodium format	H_2 production	100 mg/50 ml	231.6 mmol h^{-1}	300 W xenon lamp/(λ > 400 nm)	Wan et al. (2020)

photocatalytic systems have been one of two approaches to the splitting of H_2O into H_2 and O_2. A single particulate photo-catalyst is used to split water *via* one-stage excitation. A robust, reproducible particulate matter photo-catalyst that can be used under visible light satisfies various requirements. These include the best band gap and band position with enough driving potential. These materials also explain efficient charge-separation and conversion of electron–hole pairs, catalytic surface reduction, oxidation of water, and low corrosion. The preferred approach to achieving the two-stage excitation is well known as a Z-scheme process that is used to combine two photocatalytic with an electron transfer mediator.

Conclusion

In conclusion, we have discussed 2D g-C_3N_4-based heterostructure photocatalysts for water splitting, specifically for H_2 production. The 2D/2D interface plays a crucial role in photocatalytic H_2 production for a variety of reasons. First, the integration of 2D g-C_3N_4 with other 2D semiconductors produces a wide intimate interface which is advantageous for separating electron and hole pairs. The construction of heterostructure junctions with band structure can be employed in facilitation to separate and transport electron and hole pairs among 2D g-C_3N_4 and other 2D catalysts. The widened absorption range brought on by the synergistic interaction between 2D g-C_3N_4 and 2D semiconductors improves the utilization of sunlight. Last but not least, the establishment of an intimate contact raises the stability of photocatalysts by reducing photo corrosion and agglomeration.

Challenges and future perspective

Regardless of recent progress on the 2D g-C_3N_4-based photocatalysts, the efficacy of photocatalysts is excessively low due to the fast hole pair recombination. To overcome the current challenges, still many research efforts are needed in several aspects. First, the photocatalytic performance of 2D g-C_3N_4 can be enhanced by regulating the number of layers to obtain the significant yield of 2D photocatalyst. Second, the severe concern is agglomeration; when the different 2D components combine together, that would cause harm to the inimitable structural holes of the 2D morphology, which may hinder the photocatalytic performance. In this context, it is necessary to develop approaches to overwhelm the surface energies of 2D hetero-structures for enhanced stabilization of self-supporting in the 2D structural design. The third problem is the absence of research investigations on the thickness of 2D coating on the mode of action of heterostructures. Tentatively, the 2D structure's photocatalytic efficiencies mainly depend on the thickness. In case of electrostatic self-assembly techniques, the sacrificial reagents are normally required to attain more photocatalytic activity because of the rapid recombination of the electron–hole pairs; however, it may be in contrast with their practical uses of 2D photocatalysis. Even though the building of 2D/2D boundary by linking of 2D/2D photocatalysts may assist to deviate the charge carriers to a particular level, still more effective photogenerated charge carriers associated deviations of electron–hole pairs are extremely needed. According to future aspects, multiple interfaces are needed to explore beyond the 2D/2D interfaces for the efficient improvement of photogenerated charge carriers' segregation parallel to the interface engineering of bulk photocatalysts.

Author contributions

RM and ZA conceived and prepared the outline and supervised this review. MBH, MA, GA, and ZA helped in editing this review. SI, RR, MAA, AQ, ANC, and FZ drafted the Abstract and Introduction. RS, SZ, and Adnan helped in writing the comments. All the authors contributed to the discussion of the content and agreed to the final version of the manuscript.

Conflict of interest

The authors declare that the research was conducted in the absence of any commercial or financial relationships that could be construed as a potential conflict of interest.

Publisher's note

References

Ayodhya, D., and Veerabhadram, G. (2020). Ultrasonic synthesis of g-C_3N_4/CdS composites and their photodegradation, catalytic reduction, antioxidant and antimicrobial studies. *Mater. Res. Innovations* 24, 210–228. doi:10.1080/14328917.2019.1634356

Bard, A. J. (1979). Photoelectrochemistry and heterogeneous photo-catalysis at semiconductors. *J. Photochem.* 10, 59–75. doi:10.1016/0047-2670(79)80037-4

Cai, X., Zhang, J., Fujitsuka, M., and Majima, T. (2017a). Graphitic-C_3N_4 hybridized N-doped $La_2Ti_2O_7$ two-dimensional layered composites as efficient visible-light-driven photocatalyst. *Appl. Catal. B Environ.* 202, 191–198. doi:10.1016/j.apcatb.2016.09.021

Cai, X., Zhang, J., Fujitsuka, M., and Majima, T. (2017b). Graphitic-C_3N_4 hybridized N-doped $La_2Ti_2O_7$ two-dimensional layered composites as efficient visible-light-driven photocatalyst. *Appl. Catal. B Environ.* 202, 191–198. doi:10.1016/j.apcatb.2016.09.021

Cao, S., Shen, B., Huang, Q., and Chen, Z. (2018). Effect of sacrificial agents on the dispersion of metal cocatalysts for photocatalytic hydrogen evolution. *Appl. Surf. Sci.* 442, 361–367. doi:10.1016/j.apsusc.2018.02.105

Chen, X., and Mao, S. S. (2007). Titanium dioxide nanomaterials: Synthesis, properties, modifications, and applications. *Chem. Rev.* 107, 2891–2959. doi:10.1021/cr0500535

Dang, X., Xie, M., Dai, F., Guo, J., Liu, J., and Lu, X. (2021). Ultrathin 2D/2D $ZnIn_2S_4$/g-C_3N_4 nanosheet heterojunction with atomic-level intimate interface for photocatalytic hydrogen evolution under visible light. *Adv. Mat. Interfaces* 8, 2100151. doi:10.1002/admi.202100151

Di, J., Xia, J., Yin, S., Xu, H., Xu, L., Xu, Y., et al. (2014). Preparation of sphere-like g-C3N4/BiOI photocatalysts via a reactable ionic liquid for visible-light-driven photocatalytic degradation of pollutants. *J. Mat. Chem. A Mat.* 2, 5340. doi:10.1039/c3ta14617k

Fajrina, N., and Tahir, M. (2019). Engineering approach in stimulating photocatalytic H_2 production in a slurry and monolithic photoreactor systems using Ag-bridged Z-scheme pCN/TiO_2 nanocomposite. *Chem. Eng. J.* 374, 1076–1095. doi:10.1016/j.cej.2019.06.011

Fu, J., Xu, Q., Low, J., Jiang, C., and Yu, J. (2019). Ultrathin 2D/2D WO_3/g-C_3N_4 step-scheme H_2-production photocatalyst. *Appl. Catal. B Environ.* 243, 556–565. doi:10.1016/j.apcatb.2018.11.011

Girish, Y. R., UdayabhanuAlnaggar, G., Hezam, A., Nayan, M. B., Nagaraju, G., Byrappa, K., et al. (2022). Facile and rapid synthesis of solar-driven TiO_2/g-C_3N_4 heterostructure photocatalysts for enhanced photocatalytic activity. *J. Sci. Adv. Mater. Devices* 7, 100419. doi:10.1016/j.jsamd.2022.100419

Hao, X., Zhou, J., Cui, Z., Wang, Y., Wang, Y., and Zou, Z. (2018). Zn-vacancy mediated electron-hole separation in ZnS/g-C_3N_4 heterojunction for efficient visible-light photocatalytic hydrogen production. *Appl. Catal. B Environ.* 229, 41–51. doi:10.1016/j.apcatb.2018.02.006

Hisatomi, T., Kubota, J., and Domen, K. (2014). Recent advances in semiconductors for photocatalytic and photoelectrochemical water splitting. *Chem. Soc. Rev.* 43, 7520–7535. doi:10.1039/c3cs60378d

Hong, J., Wang, Y., Wang, Y., Zhang, W., and Xu, R. (2013). Noble-metal-free NiS/C_3N_4 for efficient photocatalytic hydrogen evolution from water. *ChemSusChem* 6, 2263–2268. doi:10.1002/cssc.201300647

Hong, Y., Fang, Z., Yin, B., Luo, B., Zhao, Y., Shi, W., et al. (2017). A visible-light-driven heterojunction for enhanced photocatalytic water splitting over Ta_2O_5 modified g-C_3N_4 photocatalyst. *Int. J. Hydrogen Energy* 42, 6738–6745. doi:10.1016/j.ijhydene.2016.12.055

Hou, Y., Laursen, A. B., Zhang, J., Zhang, G., Zhu, Y., Wang, X., et al. (2013). Layered nanojunctions for hydrogen-evolution catalysis. *Angew. Chem. Int. Ed. Engl.* 52, 3709–3713. doi:10.1002/ange.201210294

Huang, D., Li, Z., Zeng, G., Zhou, C., Xue, W., Gong, X., et al. (2019). Megamerger in photocatalytic field: 2D g-C_3N_4 nanosheets serve as support of 0D nanomaterials for improving photocatalytic performance. *Appl. Catal. B Environ.* 240, 153–173. doi:10.1016/j.apcatb.2018.08.071

Jia, J., Sun, W., Zhang, Q., Zhang, X., Hu, X., Liu, E., et al. (2020a). Inter-plane heterojunctions within 2D/2D $FeSe_2$/g-C_3N_4 nanosheet semiconductors for photocatalytic hydrogen generation. *Appl. Catal. B Environ.* 261, 118249. doi:10.1016/j.apcatb.2019.118249

Jia, J., Sun, W., Zhang, Q., Zhang, X., Hu, X., Liu, E., et al. (2020b). Inter-plane heterojunctions within 2D/2D FeSe2/g-C3N4 nanosheet semiconductors for photocatalytic hydrogen generation. *Appl. Catal. B Environ.* 261, 118249. doi:10.1016/j.apcatb.2019.118249

Li, X., Hu, J., Yang, T., Yang, X., Qu, J., and Li, C. M. (2022). Efficient photocatalytic H_2-evolution coupled with valuable furfural-production on exquisite 2D/2D $LaVO_4$/g-C_3N_4 heterostructure. *Nano Energy* 92, 106714. doi:10.1016/j.nanoen.2021.106714

Li, Z., Huang, F., Xu, Y., Yan, A., Dong, H., Luo, S., et al. (2021). 2D/2D Nb_3OF/g-C_3N_4 heterojunction photocatalysts with enhanced hydrogen evolution activity. *ACS Appl. Energy Mat.* 4, 839–845. doi:10.1021/acsaem.0c02727

Liu, C., Huang, H., Cui, W., Dong, F., and Zhang, Y. (2018). Band structure engineering and efficient charge transport in oxygen substituted g-C3N4 for superior photocatalytic hydrogen evolution. *Appl. Catal. B Environ.* 230, 115–124. doi:10.1016/j.apcatb.2018.02.038

Liu, D., Chen, D., Li, N., Xu, Q., Li, H., He, J., et al. (2020). Surface engineering of g-C3 N4 by stacked BiOBr sheets rich in oxygen vacancies for boosting photocatalytic performance. *Angew. Chem. Int. Ed. Engl.* 59, 4549–4554. doi:10.1002/ange.201914949

Liu, W., Zhang, D., Wang, R., Zhang, Z., and Qiu, S. (2022). 2D/2D interface engineering promotes charge separation of Mo_2C/g-C_3N_4 nanojunction photocatalysts for efficient photocatalytic hydrogen evolution. *ACS Appl. Mat. Interfaces* 14, 31782–31791. doi:10.1021/acsami.2c03421

Ma, L., Fan, H., Fu, K., Lei, S., Hu, Q., Huang, H., et al. (2017). Protonation of graphitic carbon nitride (g-C_3N_4) for an electrostatically self-assembling Carbon@g-C_3N_4 core–shell nanostructure toward high hydrogen evolution. *ACS Sustain. Chem. Eng.* 5, 7093–7103. doi:10.1021/acssuschemeng.7b01312

Manchala, S., Tandava, V. S. R. K., Nagappagari, L. R., Muthukonda Venkatakrishnan, S., Jampaiah, D., Sabri, Y. M., et al. (2019). Fabrication of a novel $ZnIn_2S_4$/g-C_3N_4/graphene ternary nanocomposite with enhanced charge separation for efficient photocatalytic H_2 evolution under solar light illumination. *Photochem. Photobiol. Sci.* 18, 2952–2964. doi:10.1039/c9pp00234k

Nayak, S., Mohapatra, L., and Parida, K. (2015). Visible light-driven novel g-C_3N_4/NiFe-LDH composite photocatalyst with enhanced photocatalytic activity towards water oxidation and reduction reaction. *J. Mat. Chem. A* 3, 18622–18635. doi:10.1039/c5ta05002b

Ong, W. J., Tan, L. L., Ng, Y. H., Yong, S. T., and Chai, S. P. (2016). Graphitic carbon nitride (g-C3N4)-based photocatalysts for artificial photosynthesis and environmental remediation: Are we a step closer to achieving sustainability? *Chem. Rev.* 116, 7159–7329. doi:10.1021/acs.chemrev.6b00075

Qi, Y., Chen, S., Li, M., Ding, Q., Li, Z., Cui, J., et al. (2017). Achievement of visible-light-driven Z-scheme overall water splitting using barium-modified Ta3N5as a H2-evolving photocatalyst. *Chem. Sci.* 8, 437–443. doi:10.1039/c6sc02750d

Qin, Y., Li, H., Lu, J., Feng, Y., Meng, F., Ma, C., et al. (2020). Synergy between van der waals heterojunction and vacancy in $ZnIn_2S_4$/g-C_3N_4 2D/2D photocatalysts for enhanced photocatalytic hydrogen evolution. *Appl. Catal. B Environ.* 277, 119254. doi:10.1016/j.apcatb.2020.119254

Ran, J., Guo, W., Wang, H., Zhu, B., Yu, J., and Qiao, S. Z. (2018a). Metal-free 2D/2D phosphorene/g-C_3 N_4 van der Waals heterojunction for highly enhanced visible-light photocatalytic H_2 production. *Adv. Mat.* 30, e1800128. doi:10.1002/adma.201800128

Ran, J., Guo, W., Wang, H., Zhu, B., Yu, J., and Qiao, S. Z. (2018b). Metal-free 2D/2D phosphorene/g-C3 N4 van der Waals heterojunction for highly enhanced visible-light photocatalytic H2 production. *Adv. Mat.* 30, e1800128. doi:10.1002/adma.201800128

Ran, J., Zhang, H., Fu, S., Jaroniec, M., Shan, J., Xia, B., et al. (2022). $NiPS_3$ ultrathin nanosheets as versatile platform advancing highly active photocatalytic H_2 production. *Nat. Commun.* 13, 4600. doi:10.1038/s41467-022-32256-6

She, X., Wu, J., Xu, H., Zhong, J., Wang, Y., Song, Y., et al. (2017). High efficiency photocatalytic water splitting using 2D α-Fe_2O_3/g-C_3N_4 Z-scheme catalysts. *Adv. Energy Mat.* 7, 1700025. doi:10.1002/aenm.201700025

Shen, R., Zhang, L., Chen, X., Jaroniec, M., Li, N., and Li, X. (2020). Integrating 2D/2D CdS/α-Fe_2O_3 ultrathin bilayer Z-scheme heterojunction with metallic β-NiS nanosheet-based ohmic-junction for efficient photocatalytic H_2 evolution. *Appl. Catal. B Environ.* 266, 118619. doi:10.1016/j.apcatb.2020.118619

Su, J., Li, G. D., Li, X. H., and Chen, J. S. (2019). 2D/2D heterojunctions for catalysis. *Adv. Sci.* 6, 1801702. doi:10.1002/advs.201801702

Sun, Z., Yu, Z., Liu, Y., Shi, C., Zhu, M., and Wang, A. (2019). Construction of 2D/2D $BiVO_4$/g-C_3N_4 nanosheet heterostructures with improved photocatalytic activity. *J. Colloid Interface Sci.* 533, 251–258. doi:10.1016/j.jcis.2018.08.071

Tian, Y., Chang, B., Lu, J., Fu, J., Xi, F., and Dong, X. (2013). Hydrothermal synthesis of graphitic carbon nitride-Bi_2WO_6 heterojunctions with enhanced visible light photocatalytic activities. *ACS Appl. Mat. Interfaces* 5, 7079–7085. doi:10.1021/am4013819

Tran Huu, H., Thi, M. D. N., Nguyen, V. P., Thi, L. N., Phan, T. T. T., Hoang, Q. D., et al. (2021). One-pot synthesis of S-scheme MoS_2/g-C_3N_4 heterojunction as effective visible light photocatalyst. *Sci. Rep.* 11, 14787. doi:10.1038/s41598-021-94129-0

Vinesh, V., Ashokkumar, M., and Neppolian, B. (2020). rGO supported self-assembly of 2D nano sheet of (g-C_3N_4) into rod-like nano structure and its application in sonophotocatalytic degradation of an antibiotic. *Ultrason. Sonochem.* 68, 105218. doi:10.1016/j.ultsonch.2020.105218

Wan, C., Zhou, L., Sun, L., Xu, L., Cheng, D.-G., Chen, F., et al. (2020). Boosting visible-light-driven hydrogen evolution from formic acid over AgPd/2D g-C_3N_4 nanosheets Mott-Schottky photocatalyst. *Chem. Eng. J.* 396, 125229. doi:10.1016/j.cej.2020.125229

Wang, H., Niu, R., Liu, J., Guo, S., Yang, Y., Liu, Z., et al. (2022). Electrostatic self-assembly of 2D/2D $CoWO_4$/g-C_3N_4 p—n heterojunction for improved photocatalytic hydrogen evolution: Built-in electric field modulated charge separation and mechanism unveiling. *Nano Res.* 15, 6987–6998. doi:10.1007/s12274-022-4329-z

Wang, H., Wang, B., Bian, Y., and Dai, L. (2017). Enhancing photocatalytic activity of graphitic carbon nitride by codoping with P and C for efficient hydrogen generation. *ACS Appl. Mat. Interfaces* 9, 21730–21737. doi:10.1021/acsami.7b02445

Wang, J.-C., Zhang, L., Fang, W.-X., Ren, J., Li, Y.-Y., Yao, H.-C., et al. (2015). Enhanced photoreduction CO_2 activity over direct Z-scheme α-Fe_2O_3/Cu_2O heterostructures under visible light irradiation. *ACS Appl. Mat. Interfaces* 7, 8631–8639. doi:10.1021/acsami.5b00822

Wang, J., Guan, Z., Huang, J., Li, Q., and Yang, J. (2014a). Enhanced photocatalytic mechanism for the hybrid g-C3N4/MoS2 nanocomposite. *J. Mat. Chem. A* 2, 7960–7966. doi:10.1039/c4ta00275j

Wang, J., Huang, J., Xie, H., and Qu, A. (2014b). Synthesis of g-C_3N_4/TiO_2 with enhanced photocatalytic activity for H_2 evolution by a simple method. *Int. J. Hydrogen Energy* 39, 6354–6363. doi:10.1016/j.ijhydene.2014.02.020

Wang, K., Li, Y., Li, J., and Zhang, G. (2020). Boosting interfacial charge separation of $Ba_5Nb_4O_{15}$/g-C_3N_4 photocatalysts by 2D/2D nanojunction towards efficient visible-light driven H_2 generation. *Appl. Catal. B Environ.* 263, 117730. doi:10.1016/j.apcatb.2019.05.032

Wang, X., Maeda, K., Thomas, A., Takanabe, K., Xin, G., Carlsson, J. M., et al. (2009). A metal-free polymeric photocatalyst for hydrogen production from water under visible light. *Nat. Mat.* 8, 76–80. doi:10.1038/nmat2317

Wang, Y., Shi, R., Lin, J., and Zhu, Y. (2011). Enhancement of photocurrent and photocatalytic activity of ZnO hybridized with graphite-like C3N4. *Energy Environ. Sci.* 4, 2922. doi:10.1039/c0ee00825g

Wang, Y., Wang, X., and Antonietti, M. (2012). Polymeric graphitic carbon nitride as a heterogeneous organocatalyst: From photochemistry to multipurpose catalysis to sustainable chemistry. *Angew. Chem. Int. Ed.* 51, 68–89. doi:10.1002/anie.201101182

Xu, J., Gao, J., Wang, C., Yang, Y., and Wang, L. (2017). NH_2-MIL-125(Ti)/graphitic carbon nitride heterostructure decorated with NiPd co-catalysts for efficient photocatalytic hydrogen production. *Appl. Catal. B Environ.* 219, 101–108. doi:10.1016/j.apcatb.2017.07.046

Xu, Q., Zhang, L., Cheng, B., Fan, J., and Yu, J. (2020). S-scheme heterojunction photocatalyst. *Chem* 6, 1543–1559. doi:10.1016/j.chempr.2020.06.010

Xu, Q., Zhu, B., Jiang, C., Cheng, B., and Yu, J. (2018). Constructing 2D/2D Fe_2O_3/g-C_3N_4Direct Z-scheme photocatalysts with enhanced H_2 generation performance. *Sol. RRL* 2, 1800006. doi:10.1002/solr.201800006

Yan, J., Wu, H., Chen, H., Zhang, Y., Zhang, F., and Liu, S. F. (2016). Fabrication of TiO2/C3N4 heterostructure for enhanced photocatalytic Z-scheme overall water splitting. *Appl. Catal. B Environ.* 191, 130–137. doi:10.1016/j.apcatb.2016.03.026

Yang, T., Shao, Y., Hu, J., Qu, J., Yang, X., Yang, F., et al. (2022). Ultrathin layered 2D/2D heterojunction of ReS_2/high-crystalline g-C_3N_4 for significantly improved photocatalytic hydrogen evolution. *Chem. Eng. J.* 448, 137613. doi:10.1016/j.cej.2022.137613

Yang, Y., Qiu, M., Li, L., Pi, Y., Yan, G., and Yang, L. (2018). A direct Z-scheme van der waals heterojunction (WO_3·H_2O/g-C_3N_4) for high efficient overall water splitting under visible-light. *Sol. RRL* 2, 1800148. doi:10.1002/solr.201800148

Yi, J., Fei, T., Li, L., Yu, Q., Zhang, S., Song, Y., et al. (2021). Large-scale production of ultrathin carbon nitride-based photocatalysts for high-yield hydrogen evolution. *Appl. Catal. B Environ.* 281, 119475. doi:10.1016/j.apcatb.2020.119475

Yuan, Y.-J., Shen, Z., Wu, S., Su, Y., Pei, L., Ji, Z., et al. (2019). Liquid exfoliation of g-C_3N_4 nanosheets to construct 2D-2D MoS_2/g-C_3N_4 photocatalyst for enhanced photocatalytic H_2 production activity. *Appl. Catal. B Environ.* 246, 120–128. doi:10.1016/j.apcatb.2019.01.043

Yuan, Y.-J., Yang, Y., Li, Z., Chen, D., Wu, S., Fang, G., et al. (2018). Promoting charge separation in g-C_3N_4/graphene/MoS_2 photocatalysts by two-dimensional nanojunction for enhanced photocatalytic H_2 production. *ACS Appl. Energy Mat.* 1, 1400–1407. doi:10.1021/acsaem.8b00030

Zhang, B., Hu, X., Liu, E., and Fan, J. (2021). Novel S-scheme 2D/2D BiOBr/g-C_3N_4 heterojunctions with enhanced photocatalytic activity. *Chin. J. Catal.* 42, 1519–1529. doi:10.1016/s1872-2067(20)63765-2

Zhang, H., Liu, F., Wu, H., Cao, X., Sun, J., and Lei, W. (2017). *In situ* synthesis of g-C_3N_4/TiO_2 heterostructures with enhanced photocatalytic hydrogen evolution under visible light. *RSC Adv.* 7, 40327–40333. doi:10.1039/c7ra06786k

Zhang, H., Zhu, C., Cao, J., Tang, Q., Li, M., Kang, P., et al. (2018). Ultrasonic-assisted synthesis of 2D α-Fe_2O_3@g-C_3N_4 composite with excellent visible light photocatalytic activity. *Catalysts* 8, 457. doi:10.3390/catal8100457

Zhang, S., Xu, D., Chen, X., Zhang, S., and An, C. (2020). Construction of ultrathin 2D/2D g-C_3N_4/In_2Se_3 heterojunctions with high-speed charge transfer nanochannels for promoting photocatalytic hydrogen production. *Appl. Surf. Sci.* 528, 146858. doi:10.1016/j.apsusc.2020.146858

Zhang, T., and Fu, L. (2018). Controllable chemical vapor deposition growth of two-dimensional heterostructures. *Chem* 4, 671–689. doi:10.1016/j.chempr.2017.12.006

Zhao, D., Wang, Y., Dong, C.-L., Huang, Y.-C., Chen, J., Xue, F., et al. (2021). Boron-doped nitrogen-deficient carbon nitride-based Z-scheme heterostructures for photocatalytic overall water splitting. *Nat. Energy* 6, 388–397. doi:10.1038/s41560-021-00795-9

Zheng, Y., Dong, J., Huang, C., Xia, L., Wu, Q., Xu, Q., et al. (2020). Co-doped Mo-Mo_2C cocatalyst for enhanced g-C_3N_4 photocatalytic H_2 evolution. *Appl. Catal. B Environ.* 260, 118220. doi:10.1016/j.apcatb.2019.118220

Zhong, R., Zhang, Z., Yi, H., Zeng, L., Tang, C., Huang, L., et al. (2018). Covalently bonded 2D/2D O-g-C_3N_4/TiO_2 heterojunction for enhanced visible-light photocatalytic hydrogen evolution. *Appl. Catal. B Environ.* 237, 1130–1138. doi:10.1016/j.apcatb.2017.12.066

Zhu, M., Sun, Z., Fujitsuka, M., and Majima, T. (2018). Z-scheme photocatalytic water splitting on a 2D heterostructure of black phosphorus/bismuth vanadate using visible light. *Angew. Chem. Int. Ed. Engl.* 57, 2182–2186. doi:10.1002/ange.201711357

Zou, Y., Shi, J. W., Ma, D., Fan, Z., Cheng, L., Sun, D., et al. (2018). WS_2/graphitic carbon nitride heterojunction nanosheets decorated with CdS quantum dots for photocatalytic hydrogen production. *ChemSusChem* 11, 1187–1197. doi:10.1002/cssc.201800053